



HAL
open science

Non-Hermitian skin effect in a phononic beam based on piezoelectric feedback control

Yabin Jin, Wenxin Zhong, Runcheng Cai, Xiaoying Zhuang, Yan Pennec, Bahram Djafari-Rouhani

► **To cite this version:**

Yabin Jin, Wenxin Zhong, Runcheng Cai, Xiaoying Zhuang, Yan Pennec, et al.. Non-Hermitian skin effect in a phononic beam based on piezoelectric feedback control. *Applied Physics Letters*, 2022, 121 (2), pp.022202. 10.1063/5.0097530 . hal-03742127

HAL Id: hal-03742127

<https://hal.science/hal-03742127v1>

Submitted on 7 Oct 2022


HAL is a multi-disciplinary open access archive for the deposit and dissemination of scientific research documents, whether they are published or not. The documents may come from teaching and research institutions in France or abroad, or from public or private research centers.

L'archive ouverte pluridisciplinaire **HAL**, est destinée au dépôt et à la diffusion de documents scientifiques de niveau recherche, publiés ou non, émanant des établissements d'enseignement et de recherche français ou étrangers, des laboratoires publics ou privés.

Non-Hermitian skin effect in a phononic beam based on piezoelectric feedback control

Cite as: Appl. Phys. Lett. **121**, 022202 (2022); <https://doi.org/10.1063/5.0097530>

Submitted: 29 April 2022 • Accepted: 28 June 2022 • Published Online: 12 July 2022

Yabin Jin, Wenxin Zhong,  Runcheng Cai, et al.

COLLECTIONS

Paper published as part of the special topic on [Acoustic and Elastic Metamaterials and Metasurfaces](#)



View Online



Export Citation



CrossMark

ARTICLES YOU MAY BE INTERESTED IN

[Tunable auxetic metamaterials for simultaneous attenuation of airborne sound and elastic vibrations in all directions](#)

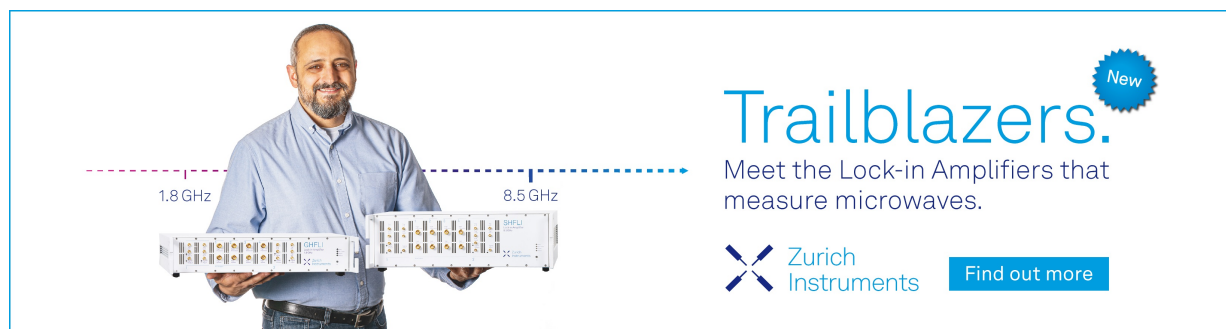
Applied Physics Letters **121**, 081702 (2022); <https://doi.org/10.1063/5.0104266>


[Inertially amplified seismic metamaterial with an ultra-low-frequency bandgap](#)

Applied Physics Letters **121**, 081701 (2022); <https://doi.org/10.1063/5.0102821>


[Non-Hermitian planar elastic metasurface for unidirectional focusing of flexural waves](#)

Applied Physics Letters **120**, 241701 (2022); <https://doi.org/10.1063/5.0097177>



Trailblazers. 

Meet the Lock-in Amplifiers that measure microwaves.

 Zurich Instruments [Find out more](#)

Non-Hermitian skin effect in a phononic beam based on piezoelectric feedback control

Cite as: Appl. Phys. Lett. **121**, 022202 (2022); doi: [10.1063/5.0097530](https://doi.org/10.1063/5.0097530)

Submitted: 29 April 2022 · Accepted: 28 June 2022 ·

Published Online: 12 July 2022



View Online



Export Citation



CrossMark

Yabin Jin,^{1,a)} Wenxin Zhong,¹ Runcheng Cai,²  Xiaoying Zhuang,^{2,3} Yan Pennec,⁴ 
and Bahram Djafari-Rouhani^{4,a)}

AFFILIATIONS

¹School of Aerospace Engineering and Applied Mechanics, Tongji University, 200092 Shanghai, China

²Department of Geotechnical Engineering, College of Civil Engineering, Tongji University, 200092 Shanghai, China

³Department of Mathematics and Physics, Institute of Photonics, Leibniz University Hannover, Hannover, Germany

⁴Département de Physique, Institut d'Electronique, de Microélectronique et de Nanotechnologie, UMR CNRS 8520, Université de Lille, 59650 Villeneuve d'Ascq, France

Note: This paper is part of the APL Special Collection on Acoustic and Elastic Metamaterials and Metasurfaces.

^{a)}Authors to whom correspondence should be addressed: 083623jinyabin@tongji.edu.cn and bahram.djafari-rouhani@univ-lille.fr

ABSTRACT

Non-Hermitian systems have gained a great deal of interest in various wave problems due their ability of exhibiting unprecedented phenomena such as invisibility, cloaking, enhanced sensing, or the skin effect. The latter manifests itself by the localization of all bulk modes in a specific frequency range at a given boundary, with an unconventional bulk-boundary correspondence. In this work, we propose to realize the skin effect for flexural waves in a non-Hermitian piezoelectric phononic beam with feedback control between a sensor and an actuator in each unit cell. By implementing a non-Hermitian parameter, effective gain and loss can be achieved in the phononic beam characterized by complex eigen frequencies, and non-reciprocal pass bands are obtained. We highlight that the split point separating the gain and loss areas can occur not only at the edges of the Brillouin zones but also inside the same Brillouin zone. We further analyze the influence of the geometric and non-Hermitian parameters on the complex dispersions and the split point. The topology of the complex bands is characterized by the winding number, which supports the skin effect together with the non-reciprocity. The localization degree of the skin mode manifested by the enhanced beam's vibration energy at one boundary is related to the strength of the non-reciprocity, and the skin mode can be always excited regardless of the source position. Our results provide a potential platform to introduce non-Hermiticity into phononic or metamaterial systems with novel functions for elastic waves such as topological insulators, vibration attenuation or amplification, and energy harvesting.

Published under an exclusive license by AIP Publishing. <https://doi.org/10.1063/5.0097530>

The Hermiticity of a Hamiltonian that describes the conservation of energy in a closed system plays a fundamental role in physics. However, actual physical systems are not always conservative since they can interact with their environment through multiphysics coupling, which can be regarded as a loss or/and gain effect to the system and result in complex eigen frequencies.¹ Non-Hermitian Hamiltonians that describe non-conservative systems were used in quantum physics.² Due to the similarity of mathematical equations between quantum and classical physics, the non-Hermitian properties have been extended to classical wave physics such as optics^{3–5} and acoustics,^{6–8} and unprecedented wave phenomena such as unidirectional invisibility,⁹ cloaking,¹⁰ enhanced sensing,¹¹ non-Hermitian skin effect,^{12–14} and coherent perfect absorption¹⁵ have been

discovered. Recently, non-Hermitian systems have been also extended to mechanical/elastic systems,^{16–21} which have rich degrees of freedom to tune non-Hermitian properties via viscosity,^{22–24} piezoelectricity,^{25–28} and so on.

Among the non-Hermitian properties, one of the most attractive phenomena is the skin effect, whereby all bulk modes of the finite chain within a specific frequency range are localized at a given boundary with an unconventional bulk-boundary correspondence,^{29,30} hence showing great potential applications such as vibration attenuation, sensing technology, and energy harvesting. This intriguing feature of the finite chain has been experimentally demonstrated with electric circuits,³¹ quantum-walk dynamics of single photons,³² among others. Recently, the non-Hermitian skin effect with such unconventional

bulk-boundary correspondence is identified in non-reciprocal mechanic metamaterial^{33,34} and in discrete elastic lattices with non-local feedback in their design.³⁵ Recently, the non-Hermitian skin effect can be also achieved via the odd micropolar elasticity.³⁶ To be mentioned, piezoelectric materials are excellent candidates to construct non-Hermitian elastic systems by means of the electro-mechanical coupling effect. The effective gain or/and loss can be realized by external non-local feedback control systems, and the non-Hermitian skin mode is achieved for longitudinal waves in a flat beam.³⁷

In this Letter, we propose a piezoelectric phononic crystal beam (Fig. 1) with a local feedback sensor and actuator in the unit cell to study non-Hermitian properties of flexural waves. By switching the feedback and tuning its strength in each unit cell, the phononic beam transforms from a Hermitian to a non-Hermitian system with non-reciprocal property in its dispersion and transmission characteristics. One obvious advantage of the proposed phononic beam is that wave attenuation and amplification in the one Brillouin zone can be obtained simply by designing the thickness ratio in the unit cell without the need for non-local feedback control. The band topology is further analyzed, and the non-Hermitian skin mode is consequently achieved. The proposed numerical design provides a potential platform for further experimental investigations.

We consider a piezoelectric phononic crystal beam made of PZT-5H with polarization along the z direction whose unit cell consists of a thin and a thick part (Fig. 1). The feedback-based unit cell is realized by employing the direct and reverse piezoelectric effect as sensors and actuators.³⁸ The rectangular cross section of the elastic beam has two symmetry planes, respectively, xOy horizontally and xOz vertically. The four types of waves in the beam (flexural, shear, torsional, and longitudinal modes) can be individually described by their symmetric or anti-symmetric behaviors with respect to the two symmetry planes.^{39–41} Following this principle, we limit ourselves to the flexural waves, which are anti-symmetric and symmetric, respectively, with respect to the xOy and xOz planes. In addition, these symmetry

considerations allow us to limit the numerical calculations to one-fourth of the unit cell, as shown in Fig. 1. We plot a full phononic beam unit and a quarter beam in blue with two middle symmetry planes in Fig. 1. Based on this symmetry principle, we consider the quarter beam for the following analysis.

The considered blue quarter unit cell is composed of a block A (as a sensor), a block B (as an actuator), and a block C with lengths $l_a = l_b = l_c = 3$ mm, widths $d_a = d_b = d_c = 1$ mm, and thicknesses $h_a = h_c = 0.4$ mm and $h_b = 0.25$ mm. To realize the feedback-based mechanism, we apply voltage to block B, and the input voltage is modulated from the detected voltage in block A.³⁵

The constitutive relations of the piezoelectric effect (displacement field and electric field) are as follows:⁴²

$$\begin{aligned} \sigma &= \mathbf{X} : \varepsilon - \mathbf{e}^T \cdot \mathbf{E}, & \varepsilon &= (\nabla \mathbf{u} + \nabla \mathbf{u}^T)/2, \\ \mathbf{D} &= \mathbf{e} : \varepsilon + \mathbf{q} \cdot \mathbf{E}, & \mathbf{E} &= -\nabla V, \end{aligned} \quad (1)$$

where σ and ε represent the stress tensor and the strain tensor, respectively, \mathbf{D} is the electric displacement vector, \mathbf{E} is the electric field vector, \mathbf{u} is the displacement vector, and V is the electric potential. \mathbf{X} , \mathbf{e} , and \mathbf{q} are the fourth-order tensor of elastic stiffness, the third-order tensor of piezoelectric modulus, and the second-order tensor of dielectric permittivity, respectively.

When the piezoelectric phononic beam vibrates, it is able to generate electric voltage. We detect the average potential difference ΔV between the upper and lower surfaces of block A then apply the average potential difference with a scale factor c as $c \Delta V$ to the upper and lower surfaces of block B. The scale factor c represents the feedback strength and also stands for the non-Hermitian parameter. Such piezoelectric feedback control systems are commonly adopted in the non-Hermitian study.^{26,27,36,37}

Now, we focus on the influence of the feedback mechanism on the dispersion relation of the piezoelectric phononic beam. First, elastic wave governing equation⁴³ and the charge conservation equation of electrostatics⁴⁴ are needed to make the piezoelectric system of equations closed. Then, we apply periodic boundary conditions to the two edges of blocks A and C along the x direction (as shown in the lower-right part of Fig. 1) by using the Bloch theorem $\mathbf{h}(\mathbf{r} + \mathbf{a}) = \mathbf{h}(\mathbf{r})e^{i\mathbf{k} \cdot \mathbf{a}}$, where \mathbf{a} , \mathbf{r} , and \mathbf{k} are the lattice size, the position vector, and the wave number, respectively. The function \mathbf{h} represents either the electric potential or the elastic displacement. Under the time-harmonic wave hypothesis, the flexural wave equation can be written in the eigenvalue equation form $(\mathbf{K} - \omega^2 \mathbf{M}) \cdot \mathbf{h} = \mathbf{0}$, where \mathbf{K} and \mathbf{M} are the generalized stiffness matrix and mass matrix, respectively. The finite element method is adopted to solve the above eigenvalue equation, and the dispersion relations can be obtained consequently.

The dispersion curves of the structure, including both the real $\text{Re}(f)$ and imaginary $\text{Im}(f)$ parts of the eigen frequencies, are presented in Fig. 2 by setting the parameter c equal to -6 . We have opted for an unfolded representation of the band diagram inside the first to fourth Brillouin zones. Clearly, all the physical information about the band diagram can also be found by using the usual folded representation only in the first Brillouin zone. However, our choice avoids to have an overlap between the curves representing the imaginary parts. The imaginary parts of the eigen frequencies in Fig. 2(b) are obtained from the general wave propagation solution of the above eigenvalue equation. To be noted that a positive or negative value of the imaginary parts of the eigen frequency $\text{Im}(f)$ means wave attenuation or

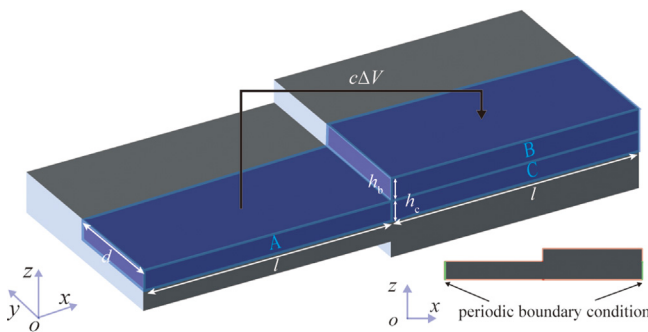


FIG. 1. Schematic of the piezoelectric phononic beam unit cell with feedback control. The structure exhibits two symmetry planes xOy and xOz . Therefore, the numerical analysis of the flexural waves, which are, respectively, anti-symmetric and symmetric with respect to these planes, can be performed by using a quarter of the unit cell. Block A is a sensor to obtain potential difference ΔV between the upper and lower surfaces generated by vibrations, and block B is an actuator to convert electric potential difference $c\Delta V$ to mechanical signals. Periodic boundary conditions are applied to the two green edges (pointed by the arrows) on blocks A and C along the x direction as shown in the lower-right part.

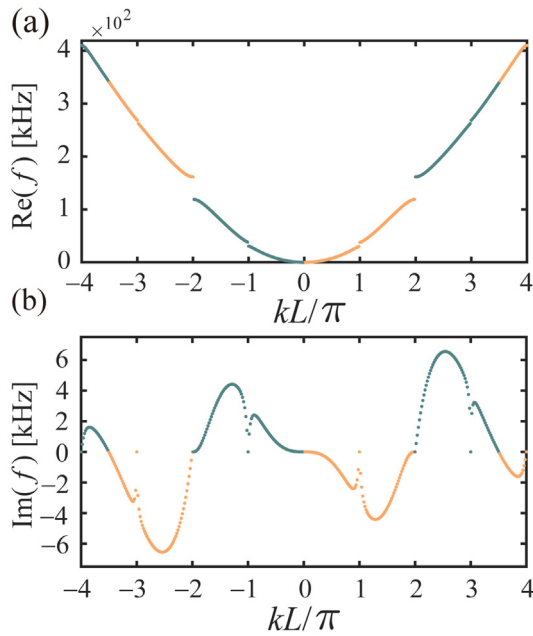


FIG. 2. Unfolded dispersion diagram of the piezoelectric unit cell: (a) real and (b) imaginary parts of eigen frequency. The green and orange colors mean that the imaginary parts of eigen frequencies are positive and negative, respectively.

amplification, respectively, the propagation direction is fixed by the sign of the wavenumber. Therefore, the curves in Fig. 2 are colored in green or yellow depending on whether $\text{Im}(f)$ is positive or negative. From Fig. 2, it can be observed that the real parts of the eigen frequencies are reciprocal, i.e., $\text{Re}(f(k)) = \text{Re}(f(-k))$, while the imaginary parts are non-reciprocal, $\text{Im}(f(k)) = -\text{Im}(f(-k))$. From the first to the third Brillouin zone, the imaginary parts of eigen frequencies are either positive or negative in each Brillouin zone. It means that the flexural wave is attenuated or amplified along a given direction within each Brillouin zone and changes its behavior when passing from one Brillouin zone to the next. However, the split point can also occur inside the same Brillouin zone as is the case in the fourth Brillouin zone. The latter is split into a positive and a negative region where the split point corresponds to $\text{Re}(f) = 340\text{Hz}$. This feature is also observed in a longitudinal waveguide controlled by the non-local feedback mechanism (where the feedback force obtained from one unit is applied to another unit).³⁷

From the dispersion curves in Fig. 2, we demonstrate that the passband of the unit cell is completely non-reciprocal due to the opposite sign of $\text{Im}(f(k))$ for positive and negative k . In order to confirm the non-reciprocal behavior and the meaning of attenuation or amplification, we show the unfolded dispersions over the first four Brillouin zones with the corresponding transmission along positive and negative wavevector directions in the upper and lower panels of Fig. 3, respectively. The transmission diagram is divided into horizontal areas that are colored according to the color on the dispersion curves. We plot both $\log(T)$ and $\log(R + T)$ in Figs. 3(b) and 3(d) with T and R being the square modulus of the transmission and reflection coefficients of a finite piezoelectric beam, respectively. It is obviously confirmed that the transmission is completely non-reciprocal due to the big value

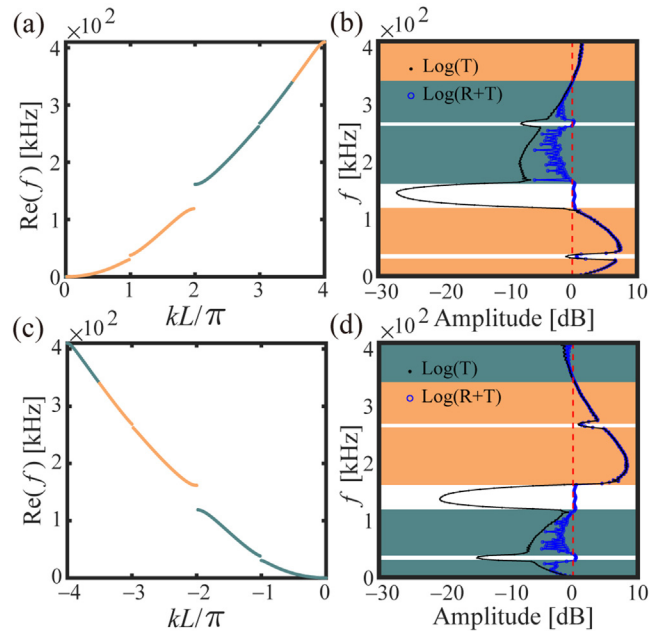


FIG. 3. (a) Real parts of the eigen frequencies in the dispersion curves of Fig. 2 for positive wavenumbers. (b) The corresponding $\log(T)$ and $\log(R + T)$ curves. (c) and (d) The same plots as the upper panels for negative wavenumbers. The green and orange regions indicate wave attenuation and amplification, respectively.

difference in $\log(T)$ from Figs. 3(b) and 3(d). In addition, the attenuation (green) or amplified (orange) effects are also confirmed by the sign of $\log(R + T)$.

The non-Hermitian skin effect associated with flexural waves can be determined from the topology of the complex band structure via the winding number ν .^{45–47} The winding number ν can be evaluated by simply counting the number of loops, which is necessary to achieve a closed curve when increasing the wavenumber in each Brillouin zone. If c is zero, the system is Hermitian, and the eigen frequencies are purely real; then, the number of loop is zero, so is the winding number,⁴⁵ showing a trivial character of the bands. In Fig. 4(a), we plot the complex band diagram when the feedback strength c is fixed to -6 . The four pass bands are marked by yellow, blue, purple, and red dots. Their projections on the complex frequency plane form loops as shown in Fig. 4(b). The arrow on each loop indicates the direction of increasing wavenumber k corresponding to the sign of the winding number ν , i.e., clockwise for $\nu = -1$ and anticlockwise for $\nu = 1$.⁴⁵

From Fig. 4(b), the four pass bands in Fig. 2 have five loops on the complex frequency plane, and each loop closes after one 2π rotation. The highlighted green and orange loops have clockwise and anticlockwise arrows, which correspond to winding number $\nu = -1$ and $\nu = 1$, respectively. For the orange zones I, II, and V, the propagation of flexural waves to the right ($+x$ direction) is amplified, meaning that all bulk modes of the finite periodic beam whose eigen frequencies lie inside the orange zone are localized at the right boundary of the beam; on the contrary, the green zones III and IV correspond to eigenmode localization at the left boundary of the beam. It should be noted that if the scale factor c is chosen as 6 instead of -6 , the boundary where the

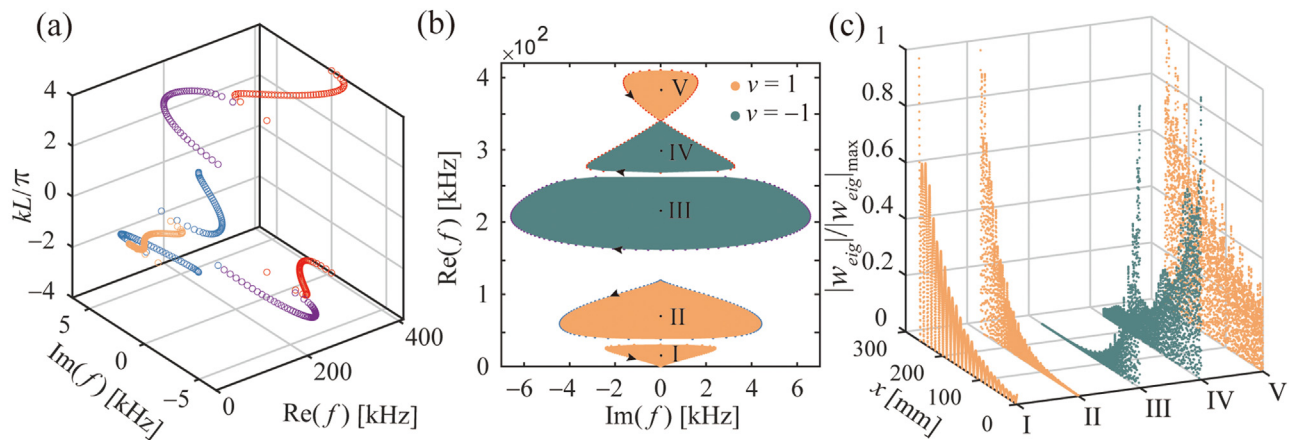


FIG. 4. Topology of dispersion bands and the non-Hermitian skin effect in phononic beam. (a) The complex dispersion band with $c = -6$. The four pass bands are represented by yellow, blue, purple, and red dots. (b) Projection of the complex dispersion band on the complex eigen frequency plane. The projected orange and green loops with anticlockwise and clockwise arrows correspond to the winding number $\nu = 1$ and $\nu = -1$, respectively. (c) The normalized vertical displacement component of the skin eigenmodes in a beam consisting of 44 unit cells, at the eigen frequencies corresponding to the black dots in each loop.

modes are localized will be inverted between zones (I, II, and V) and zones (III and IV).

We further consider a beam of finite length consisting of 44 units and calculate the corresponding eigen frequencies that will fall inside the five loops. The number of unit cells should be chosen in order to clearly identify the skin effect (as shown below), and in our case, a satisfactory number would be in the range of 40–50. We choose one eigen frequency, marked as a black dot at the center of each closed loop in Fig. 4(b) and plot in Fig. 4(c) its eigenmode, namely, the normalized vertical displacement along the x axis of the beam. When $\nu = 1$ (orange zones I, II, V), the displacement is localized at the right boundary, while for $\nu = -1$ (green zones III and IV), the localization occurs at the left boundary. For the eigen frequency chosen in loop III, the imaginary part is large, which explains the big difference in transmission in Figs. 3(c) and 3(f), indicating a strong non-reciprocity. Therefore, the corresponding non-Hermitian skin mode III in Fig. 4(c) is highly localized at the left boundary. For the non-Hermitian skin mode V, the imaginary parts of the eigen frequency are small, resulting in a small difference in transmission in Figs. 3(c) and 3(f), a weak non-reciprocity, and a weak displacement localization at the right boundary. It should be mentioned that the non-Hermitian skin effect can be observed for all eigenmodes belonging to each of the five loops.

In addition, one can again highlight the split point in the imaginary parts of the eigen frequency in the fourth Brillouin zone, at the crossing of loops IV and V.

Finally, we have further checked that the non-Hermitian skin effect can also appear when the boundary condition at both ends of the beam is changed from free to fixed.

In order to have a deeper insight about the designed non-Hermitian phononic beam, we study in Fig. 5 the evolution of the complex band structure as a function of two parameters in the system, namely, the thickness h of block B and the non-Hermitian scale factor c . First, we keep the non-Hermitian parameter $c = -6$ fixed and select three values of the block B's thickness h as $h = 0.1, 0.25,$ and 0.4 mm [see Figs. 5(a)–5(c), respectively]. Obviously, all five loops change

shapes as well as the bandgaps. When increasing h , the maximum absolute value of $\text{Im}(f)$ will decrease for the first three loops; the fourth loop becomes smaller and the fifth loop widens. In addition, the split point connecting the fourth and fifth loops downshifts in frequency. Then, we keep $h = 0.25$ mm fixed and vary c from -4 to -8 [Figs. 5(d)–5(f)]. When increasing the absolute value of c , the maximum absolute value of $\text{Im}(f)$ will increase for all the five loops since the non-Hermitian strength becomes stronger. The split point connecting the fourth and fifth loops remains stable.

As analyzed above, the non-Hermitian skin mode is highly related to the strength of non-reciprocity. One essential property of the non-Hermitian skin mode is that the flexural wave can always propagate with an amplification factor along one direction, while the propagation in opposite direction can be suppressed with an attenuation factor. Therefore, the non-Hermitian skin mode is independent of the position of the excitation source on the beam.⁴⁸ In order to validate this statement, we calculate the transmission along a finite phononic beam consisting of 44 units (with free boundary condition) with three excitation sources at 10 kHz located, respectively, at the left (green), middle (blue), and right (red) of the beam, as shown in the inset of Fig. 6. The normalized vertical displacement distributions along the finite phononic beam are plotted in Fig. 6, which clearly support that the displacements are always localized at the right boundary regardless of the excitation position.

To summarize, we proposed a non-Hermitian phononic beam with feedback control via the direct and inverse piezoelectric effects. Switching the non-Hermitian parameter of the feedback control in the unit cell, effective gain and loss are obtained, which are characterized by the imaginary part of the eigen frequencies, and non-reciprocity is achieved for flexural waves in both dispersion curves and transmission diagrams. In the first three Brillouin zones, the non-Hermitian phononic beam exhibits either gain or loss effect, while in the fourth Brillouin zone, there is a split point from gain to loss. We have analyzed the influence of the Block B's thickness and the non-Hermitian parameter on the complex band structure and the split point. We characterized the topology of complex bands by their winding

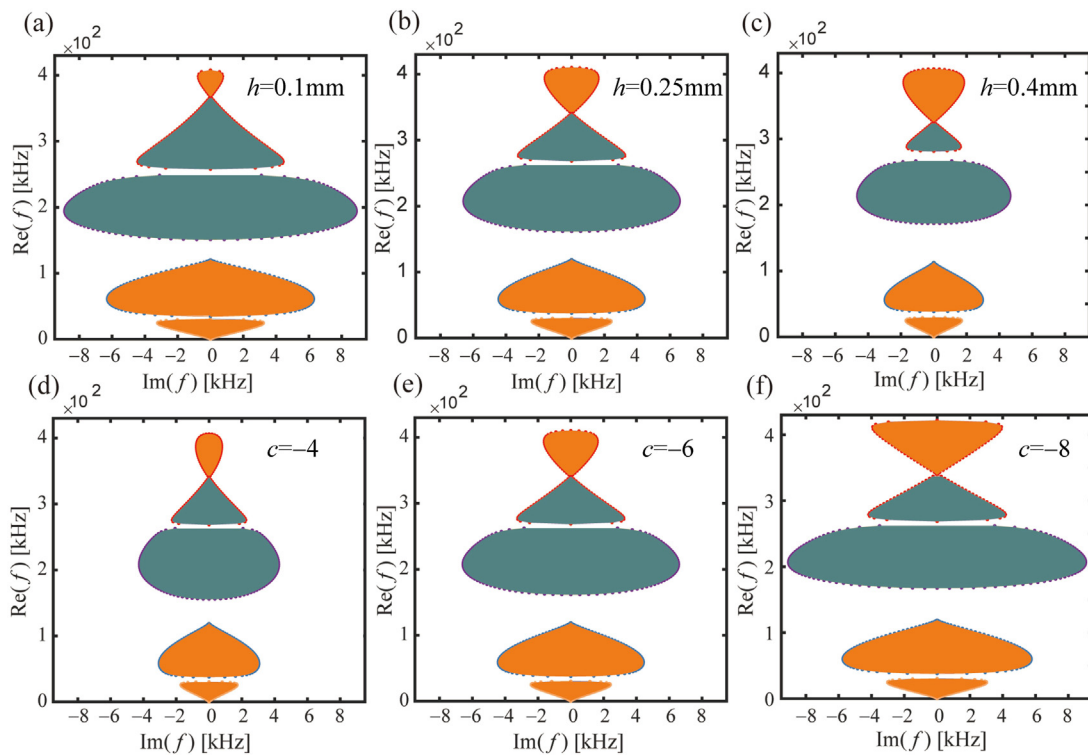


FIG. 5. The influence of (a)–(c) Block B's thickness h and (d)–(f) non-Hermitian parameter c on the complex dispersion projection.

numbers, showing non-trivial properties of the pass bands. Thanks to the non-reciprocal and non-trivial nature of the spectrum, the proposed non-Hermitian elastic system exhibits the skin effect to localize vibrating energy at one boundary in a finite phononic beam. The energy localization direction and strength of the non-Hermitian skin effect can be determined by the sign of the non-Hermitian parameter

and the non-reciprocal strength, respectively. To further validate the skin mode design, we change the polarization of the PZT material from the z direction to the y direction and show a feasible skin effect in the [supplementary material](#). The proposed strategy where non-Hermitian property is introduced into the phononic structures paves the way toward a feasible non-Hermitian elastic platform for promising applications such as sensing, vibration control, or energy harvesting.

See the [supplementary material](#) for details of another scheme to obtain the feasible skin effect.

This work was supported by the National Natural Science Foundation of China (No. 11902223), the Young Elite Scientists Sponsorship Program by CAST (No. 2021QNRC001), the Shanghai Science and Technology Committee (Grant No. 21JC1405600), the program for professor of special appointment (Eastern Scholar) at Shanghai Institutions of Higher Learning, and the Fundamental Research Funds for the Central Universities.

AUTHOR DECLARATIONS

Conflict of Interest

The authors have no conflicts to disclose.

Author Contributions

Yabin Jin: Conceptualization (lead); Funding acquisition (lead); Investigation (equal); Resources (lead); Supervision (lead); Writing – original draft (equal); Writing – review and editing (equal). **Wenxin**

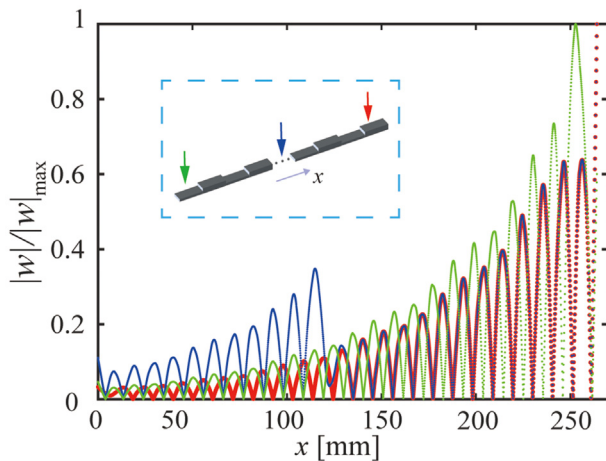


FIG. 6. The normalized vertical displacement distributions along the finite phononic beam with free boundary conditions for three excitation sources at 10 kHz at the left (green), middle (blue), or right (red) as marked in the insert. The blue and red curves are merged on the right half of the beam.

Zhong: Data curation (equal); Formal analysis (equal); Investigation (equal); Methodology (equal); Software (equal); Validation (equal); Visualization (equal); Writing – original draft (equal); Writing – review and editing (equal). **Runcheng Cai:** Formal analysis (equal); Investigation (equal); Methodology (equal); Software (equal); Validation (equal); Visualization (equal); Writing – original draft (equal); Writing – review and editing (equal). **Xiaoying Zhuang:** Methodology (equal); Writing – original draft (equal); Writing – review and editing (equal). **Yan Pennec:** Methodology (equal); Writing – original draft (equal); Writing – review and editing (equal). **Bahram Djafari-Rouhani:** Formal analysis (equal); Investigation (equal); Supervision (equal); Writing – original draft (equal); Writing – review and editing (equal).

DATA AVAILABILITY

The data that support the findings of this study are available from the corresponding authors upon reasonable request.

REFERENCES

- ¹Z. Gu, H. Gao, P.-C. Cao, T. Liu, X.-F. Zhu, and J. Zhu, “Controlling sound in non-Hermitian acoustic systems,” *Phys. Rev. Appl.* **16**, 057001 (2021).
- ²I. Rotter, “A non-Hermitian Hamilton operator and the physics of open quantum systems,” *J. Phys. A: Math. Theor.* **42**, 153001 (2009).
- ³L. Lu, J. D. Joannopoulos, and M. Soljačić, “Topological photonics,” *Nat. Photonics* **8**, 821–829 (2014).
- ⁴R. El-Ganainy, K. G. Makris, M. Khajavikhan, Z. H. Musslimani, S. Rotter, and D. N. Christodoulides, “Non-Hermitian physics and PT symmetry,” *Nat. Phys.* **14**, 11–19 (2018).
- ⁵S. Longhi, “Parity-time symmetry meets photonics: A new twist in non-Hermitian optics,” *Europhys. Lett.* **120**, 64001 (2017).
- ⁶V. Achilleos, G. Theocharis, O. Richoux, and V. Pagneux, “Non-Hermitian acoustic metamaterials: Role of exceptional points in sound absorption,” *Phys. Rev. B* **95**, 144303 (2017).
- ⁷N. Gerard and Y. Jing, “Loss in acoustic metasurfaces: A blessing in disguise,” *MRS Commun.* **10**, 32–41 (2020).
- ⁸Y. Auregan and V. Pagneux, “PT-symmetric scattering in flow duct acoustics,” *Phys. Rev. Lett.* **118**, 174301 (2017).
- ⁹L. Feng, Y. L. Xu, W. S. Fegadolli, M. H. Lu, J. E. Oliveira, V. R. Almeida, Y. F. Chen, and A. Scherer, “Experimental demonstration of a unidirectional reflectionless parity-time metamaterial at optical frequencies,” *Nat. Mater.* **12**, 108–113 (2013).
- ¹⁰S. A. Cummer and D. Schurig, “One path to acoustic cloaking,” *New J. Phys.* **9**, 45–45 (2007).
- ¹¹Q. Zhong, J. Ren, M. Khajavikhan, D. N. Christodoulides, S. K. Ozdemir, and R. El-Ganainy, “Sensing with exceptional surfaces in order to combine sensitivity with robustness,” *Phys. Rev. Lett.* **122**, 153902 (2019).
- ¹²X. Zhang, Y. Tian, J. H. Jiang, M. H. Lu, and Y. F. Chen, “Observation of higher-order non-Hermitian skin effect,” *Nat. Commun.* **12**, 5377 (2021).
- ¹³P.-C. Cao, Y.-G. Peng, Y. Li, and X.-F. Zhu, “Phase-locking diffusive skin effect,” *Chin. Phys. Lett.* **39**, 057801 (2022).
- ¹⁴P.-C. Cao, Y. Li, Y.-G. Peng, M. Qi, W.-X. Huang, P.-Q. Li, and X.-F. Zhu, “Diffusive skin effect and topological heat funneling,” *Commun. Phys.* **4**, 230 (2021).
- ¹⁵K. Pichler, M. Kuhmayer, J. Bohm, A. Brandstotter, P. Ambichl, U. Kuhl, and S. Rotter, “Random anti-lasing through coherent perfect absorption in a disordered medium,” *Nature* **567**, 351–355 (2019).
- ¹⁶J. Yi, Z. Li, M. Negahban, R. Xia, and J. Zhu, “Asymmetric viscoelastic metamaterials for broad bandgap design and unidirectional zero reflection,” *Mech. Syst. Signal Process.* **162**, 108101 (2022).
- ¹⁷M. Farhat, P. Y. Chen, S. Guenneau, and Y. Wu, “Self-dual singularity through lasing and antilasing in thin elastic plates,” *Phys. Rev. B* **103**, 134101 (2021).
- ¹⁸M. I. N. Rosa, M. Mazzotti, and M. Ruzzene, “Exceptional points and enhanced sensitivity in PT-symmetric continuous elastic media,” *J. Mech. Phys. Solids* **149**, 104325 (2021).
- ¹⁹Y. Jin, Y. Pennec, B. Bonello, H. Honarvar, L. Dobrzynski, B. Djafari-Rouhani, and M. I. Hussein, “Physics of surface vibrational resonances: Pillared phononic crystals, metamaterials, and metasurfaces,” *Rep. Prog. Phys.* **84**, 086502 (2021).
- ²⁰Y. Jin, L. He, Z. Wen, B. Mortazavi, H. Guo, D. Torrent, B. Djafari-Rouhani, T. Rabczuk, X. Zhuang, and Y. Li, “Intelligent on-demand design of phononic metamaterials,” *Nanophotonics* **11**, 439–460 (2022).
- ²¹Z. Wen, W. Wang, A. Khelif, B. Djafari-Rouhani, and Y. Jin, “A perspective on elastic metastructures for energy harvesting,” *Appl. Phys. Lett.* **120**, 020501 (2022).
- ²²E. Ghavanloo and M. Shaat, “General nonlocal Kelvin–Voigt viscoelasticity: Application to wave propagation in viscoelastic media,” *Acta Mech.* **233**, 57–67 (2022).
- ²³X. Li, Z. Yu, H. Iizuka, and T. Lee, “Experimental demonstration of extremely asymmetric flexural wave absorption at the exceptional point,” *Extreme Mech. Lett.* **52**, 101649 (2022).
- ²⁴Y. Liu, Z. Liang, J. Zhu, L. Xia, O. Mondain-Monval, T. Brunet, A. Alù, and J. Li, “Willis metamaterial on a structured beam,” *Phys. Rev. X* **9**, 011040 (2019).
- ²⁵Q. Wu, X. Zhang, P. Shivashankar, Y. Chen, and G. Huang, “Independent flexural wave frequency conversion by a linear active metalayer,” *Phys. Rev. Lett.* **128**, 244301 (2022).
- ²⁶Q. Wu, Y. Chen, and G. Huang, “Asymmetric scattering of flexural waves in a parity-time symmetric metamaterial beam,” *J. Acoust. Soc. Am.* **146**, 850–862 (2019).
- ²⁷Z. Hou and B. Assouar, “Tunable elastic parity-time symmetric structure based on the shunted piezoelectric materials,” *J. Appl. Phys.* **123**, 085101 (2018).
- ²⁸Z. Hou, H. Ni, and B. Assouar, “PT-symmetry for elastic negative refraction,” *Phys. Rev. Appl.* **10**, 044071 (2018).
- ²⁹S. Yao and Z. Wang, “Edge states and topological invariants of non-Hermitian systems,” *Phys. Rev. Lett.* **121**, 086803 (2018).
- ³⁰F. K. Kunst, E. Edvardsson, J. C. Budich, and E. J. Bergholtz, “Biorthogonal bulk-boundary correspondence in non-Hermitian systems,” *Phys. Rev. Lett.* **121**, 026808 (2018).
- ³¹S. Liu, R. Shao, S. Ma, L. Zhang, O. You, H. Wu, Y. J. Xiang, T. J. Cui, and S. Zhang, “Non-Hermitian skin effect in a non-Hermitian electrical circuit,” *Research* **2021**, 5608038.
- ³²L. Xiao, T. Deng, K. Wang, G. Zhu, Z. Wang, W. Yi, and P. Xue, “Non-Hermitian bulk-boundary correspondence in quantum dynamics,” *Nat. Phys.* **16**, 761–766 (2020).
- ³³M. Brandenbourger, X. Locsin, E. Lerner, and C. Coulais, “Non-reciprocal robotic metamaterials,” *Nat. Commun.* **10**, 4608 (2019).
- ³⁴A. Ghatak, M. Brandenbourger, J. van Wezel, and C. Coulais, “Observation of non-Hermitian topology and its bulk-edge correspondence in an active mechanical metamaterial,” *Proc. Natl. Acad. Sci.* **117**, 29561–29568 (2020).
- ³⁵M. I. N. Rosa and M. Ruzzene, “Dynamics and topology of non-Hermitian elastic lattices with non-local feedback control interactions,” *New J. Phys.* **22**, 053004 (2020).
- ³⁶Y. Chen, X. Li, C. Scheibner, V. Vitelli, and G. Huang, “Realization of active metamaterials with odd micropolar elasticity,” *Nat. Commun.* **12**, 5935 (2021).
- ³⁷D. Braghini, L. G. G. Villani, M. I. N. Rosa, and J. R. de F. Arruda, “Non-Hermitian elastic waveguides with piezoelectric feedback actuation: Non-reciprocal bands and skin modes,” *J. Phys. D: Appl. Phys.* **54**, 285302 (2021).
- ³⁸L. Li and Y. Guo, “Analysis of longitudinal waves in rod-type piezoelectric phononic crystals,” *Crystals* **6**, 45 (2016).
- ³⁹Y. Jin, W. Wang, and B. Djafari-Rouhani, “Asymmetric topological state in an elastic beam based on symmetry principle,” *Int. J. Mech. Sci.* **186**, 105897 (2020).
- ⁴⁰W. Wang, Y. Jin, W. Wang, B. Bonello, B. Djafari-Rouhani, and R. Fleury, “Robust Fano resonance in a topological mechanical beam,” *Phys. Rev. B* **101**, 024101 (2020).
- ⁴¹L. He, H. Guo, Y. Jin, X. Zhuang, T. Rabczuk, and Y. Li, “Machine-learning-driven on-demand design of phononic beams,” *Sci. China Phys., Mech. Astron.* **65**, 214612 (2022).
- ⁴²D. Ammosov, M. Vasilyeva, A. Nasedkin, and Y. Efendiev, “Generalized multi-scale finite element method for piezoelectric problem in heterogeneous media,” *Eng. Anal. Boundary Elem.* **135**, 12–25 (2022).

- ⁴³X. Wu, Z. Wen, Y. Jin, T. Rabczuk, X. Zhuang, and B. Djafari-Rouhani, "Broadband Rayleigh wave attenuation by gradient metamaterials," *Int. J. Mech. Sci.* **205**, 106592 (2021).
- ⁴⁴X. Dai, F. Zhu, Z. Qian, and J. Yang, "Electric potential and carrier distribution in a piezoelectric semiconductor nanowire in time-harmonic bending vibration," *Nano Energy* **43**, 22–28 (2018).
- ⁴⁵Z. Gong, Y. Ashida, K. Kawabata, K. Takasan, S. Higashikawa, and M. Ueda, "Topological phases of non-Hermitian systems," *Phys. Rev. X* **8**, 031079 (2018).
- ⁴⁶T. Kitagawa, E. Berg, M. Rudner, and E. Demler, "Topological characterization of periodically driven quantum systems," *Phys. Rev. B* **82**, 235114 (2010).
- ⁴⁷C. Yin, H. Jiang, L. Li, R. Lü, and S. Chen, "Geometrical meaning of winding number and its characterization of topological phases in one-dimensional chiral non-Hermitian systems," *Phys. Rev. A* **97**, 052115 (2018).
- ⁴⁸S. Mandal, R. Banerjee, and T. C. Liew, "From the topological spin-Hall effect to the non-Hermitian skin effect in an elliptical micropillar chain," *ACS Photonics* **9**, 527–539 (2022).